RSC Advances

PAPER

View Article Online
View Journal | View Issue

Cite this: *RSC Adv.*, 2015, **5**, 25896

Efficient removal of hexavalent chromium by high surface area Al_2O_3 rods

Xiang-Qian Zhang, Yue Guo and Wen-Cui Li*

Received 24th December 2014
Accepted 2nd March 2015

DOI: 10.1039/c4ra16953k

www.rsc.org/advances

Rod-like alumina materials were synthesized *via* a template-free hydrothermal method by using aluminum nitrate as precursor and urea as precipitating agent. The resulting alumina has a high specific surface area (up to 773 $m^2\ g^{-1}$) and an abundance of hydroxyl groups, giving it a good Cr(VI) removal efficiency. External factors were investigated, including contact time, adsorbent dose, initial concentration of adsorbate and pH. The maximum adsorption capacity for Cr(VI) was 39.1 mg g^{-1}, which is superior to most of the reported alumina adsorbents. The Al_2O_3 samples before and after Cr(VI) adsorption were also characterized by FT-IR and XPS analysis. The results show that the adsorption can be mainly ascribed to the ion exchange between the abundant hydroxyl groups on the alumina surface and chromium anions. Together with an outstanding adsorption–regeneration performance, it is anticipated that the as-synthesized alumina materials are an attractive adsorbent for the removal of heavy metal ions from water.

1. Introduction

The increasing heavy metal contamination in groundwater and drinking water has become one of the key environmental health problems facing humanity.[1,2] Hexavalent chromium (Cr(VI)) is a great concern due to its extreme toxicity and carcinogenicity to living organisms. It also has been designated as one of the top-priority toxic pollutants by the U.S. Environmental Protection Agency (EPA).[3–6] However, chromium is widely used in a variety of industrial applications as large quantities of chromium are being discharged into the environment. Thus, it is necessary to develop simple and effective methods to remove Cr(VI) from aqueous solution streams, in order to avoid a deleterious impact on human health.

During recent years, many treatment processes[1,7,8] have been carried out for heavy metal ion removal such as adsorption, precipitation, membrane filtration, reverse osmosis, biological treatment and ion-exchange. Adsorption method has been widely investigated owing to its feasibility and economic viability.[9–12] Up to date, various porous metal oxides including aluminum oxides,[13,14] iron oxides,[15–17] cerium oxides,[18,19] and titanium oxides[17,20] have been studied for Cr(VI) removal. Among them, aluminum oxides with large surface area, well-defined porosity and abundant surface functional groups have been regarded as an attractive adsorbent material for water treatment.[1,2,9,21] Additionally, the strong resistance to thermal degradation of alumina and large-scale production also make this non-hazardous material an excellent candidate for water decontamination.[22]

Up to now, several approaches have been reported in this direction utilizing Al_2O_3 materials and their composites as adsorbent for removal of Cr(VI) from aqueous solutions. As previously reported in the literatures, considerable attention has been paid to the synthesis of hierarchically structured materials whose hierarchical nanometer-sized building blocks are expected to provide a high surface-to-bulk ratio and surface functional groups. For example, a mesoporous γ-Al_2O_3 with unique hierarchical structure was fabricated by a non-template hydrothermal synthesis, which exhibited a adsorption capacity of ~6.7 mg g^{-1} for Cr(VI).[23] Moreover, the application of nanoparticles as adsorbents has come up as an interesting area of research and they are considered to show high removal efficiency because of their nanosize and a high surface area, which may provide a greater number of active sites to interact with the pollutant species. Inspired by this, Sharma *et al.* used the facile sol–gel method to prepare nano-Al_2O_3 powder and the average crystallite size was determined to be in the range of 15 to 20 nm by XRD and TEM analysis.[24] However, the maximum adsorption capacity for Cr(VI) was only 8.56 mg g^{-1}, which may be due to the undesirable specific surface area (S_{BET}) of 78.79 $m^2\ g^{-1}$. The Cr(VI) removal performance of those reported materials still need to be enhanced.

Therefore, it is urgent to explore an efficient alumina adsorbent having a desirable surface area, high adsorption capacity and good recyclability. In this work, we report a high surface area alumina material through a simple hydrothermal process followed by a calcination step using aluminum nitrate as precursor and urea as precipitator without any template. The final alumina products show a rod-like morphology with a high surface area of up to 773 $m^2\ g^{-1}$ and an abundance of hydroxyl groups. The Cr(VI) removal performance was studied with an

State Key Laboratory of Fine Chemicals, School of Chemical Engineering, Dalian University of Technology, China. E-mail: wencuili@dlut.edu.cn

emphasis on the adsorption kinetics and the adsorption mechanism in order to better understand the adsorbate–adsorbent systems. The preliminary study about the adsorbent's stability of adsorption–regeneration has also been carried out in the current work.

2. Experimental

2.1 Materials

$Al(NO_3)_3 \cdot 9H_2O$ was purchased from Shanghai Xinbao Fine Chemical Factory. $CO(NH_2)_2$ was purchased from Tianjin Kemiou Chemical Reagent Co., Ltd. Potassium dichromate ($K_2Cr_2O_7$) was purchased from Sinopharm Chemical Reagent Co., Ltd. Stock solution of Cr(VI) was prepared by dissolving $K_2Cr_2O_7$ in distilled water. All other chemicals used in this study were of analytical grade and without any further purification.

2.2 The preparation of porous alumina

The alumina materials were prepared using $Al(NO_3)_3 \cdot 9H_2O$ as precursor and urea as precipitant under hydrothermal conditions followed by a calcination step inspired by our previous work.[25–27] A typical procedure was as follows: $Al(NO_3)_3 \cdot 9H_2O$ (0.0185 mol) was dissolved in deionized water (30 mL), and $CO(NH_2)_2$ (0.167 mol) was then added to form a mixed solution under vigorous stirring for 10 min at 25 °C. Subsequently, the obtained homogeneous solution was transferred into a Teflon-lined stainless steel autoclave and maintained at 100 °C for 24 h, and then cooled to room temperature. The white precipitate was filtered off, washed with deionized water and anhydrous alcohol, then dried at 80 °C for 12 h, followed by calcination at the designate temperature (300, 500, or 700 °C) for 2 h. Samples have been named as Al-*x*, where *x* represents the calcinations temperature.

2.3 Characterization

The microscopic features of the samples were characterized by scanning electron microscopy (SEM) with an S4800 instrument. Fourier transform-infrared (FT-IR) spectra were recorded on a Nicolet 6700 FT-IR spectrometer with the samples pressed into KBr discs. X-ray diffraction patterns (XRD) were obtained with a D/MAX-2400 diffractometer using Cu Kα radiation (40 kV, 100 mA, $\lambda = 1.54056$ Å). Thermogravimetric and differential scanning calorimetry analyses (TG-DSC) were conducted on a thermogravimetric analyzer STA 449 F3 (NETZSCH), under an air atmosphere with a heating rate of 10 °C min^{-1}. X-ray photoelectron spectroscopy (XPS) measurements were performed on an ESCALAB 250Xi (Thermo Scientific, USA) using monochromatic Al Kα excitation source. Binding energies were corrected for surface charging by referencing them to the energy of the C 1s peak of the contaminant carbon at 284.6 eV. The textural characterizations of the samples were performed by nitrogen sorption at 77 K using a Micromeritics Instrument Corporation Tristar 3000 device. Prior to the measurements, the samples were degassed at 473 K for 4 h. Surface areas (S_{BET}) were calculated using the Brunauer–Emmett–Teller (BET) method and pore size distributions (PSDs) were derived from the adsorption branches of the isotherms using the Barrett–Joyner–Halenda (BJH) model. Total pore volumes (V_{total}) were calculated from the amount adsorbed at a relative pressure (P/P_0) of 0.995.

2.4 Determination of hydroxyl groups concentration on alumina

The density of surface hydroxyl groups on alumina was calculated by fluoride ion adsorption.[28] Typically, 50 mg alumina was added to 20 mL of NaF (420 mg L^{-1}) solution, whose pH was adjusted to 4.6 using an acetic acid (0.2 mol L^{-1})–sodium acetate (0.2 mol L^{-1}) buffer, and shaken for 24 h. The density of hydroxyl groups was calculated from the difference between the initial and equilibrium fluoride ion concentrations measured using a UV-Vis spectrophotometer at a wavelength of 620 nm.

2.5 Adsorption measurements

The obtained Al_2O_3 samples were used to remove Cr(VI) from aqueous solutions according to the reported method.[12,29] A stock solution of Cr(VI) (100 mg L^{-1}) was prepared in deionized water using $K_2Cr_2O_7$ as the source of Cr(VI). HCl solution (pH = 1.0) was used for pH adjustment. Typically, the batch experiments were carried out with a certain concentration of Cr(VI) (30 mL) and adsorbent were added into a flask. Here, the adsorbent dose was 2 g L^{-1} in all experiments except the studies on the adsorbent dose. After a specified time interval of adsorption at 25 °C, the Cr(VI) solutions were withdrawn by a syringe-driven filter. The Cr(VI) concentrations were measured using a UV2300 UV-Vis spectrophotometer at $\lambda = 540$ nm with 1,5-diphenylcarbazide.

The removal efficiency of Cr(VI) (%) and the adsorption capacity q_t (mg g^{-1}) was calculated by eqn (1) and (2):

$$\text{Removal efficiency of Cr(VI)} = \frac{(C_0 - C_t)}{C_0} \times 100\% \quad (1)$$

$$q_e = \frac{(C_0 - C_e)V}{M} \quad (2)$$

where, C_0 and C_e are the initial and equilibrium concentrations (mg L^{-1}), respectively and C_t is the corresponding concentrations (mg L^{-1}) after time *t* of the Cr(VI) solutions. *M* is the mass of the adsorbent (g), and *V* is the volume of the solution (*L*).

2.6 Adsorption–regeneration for recycling

In the present work, saturated KCl solution was used for the regeneration of the adsorbent. In detail, 0.1 g Cr-loaded adsorbent was added to 23 mL of KCl solution and agitated for 24 h at 25 °C. Then the eluted adsorbent was separated from the KCl solution, washed thoroughly with water, followed by drying at 50 °C in air. The recycling experiment was conducted by using the regenerative adsorbent to remove Cr(VI) from fresh Cr(VI) aqueous solutions.

2.7 Adsorption kinetics and isotherms

The Ho's pseudo-second-order model was employed to study the adsorption process for Cr(VI), as expressed by eqn (3).

$$\frac{t}{q_t} = \frac{1}{k_2 q_e^2} + \frac{t}{q_e} \quad (3)$$

where, q_e and q_t(mg g^{-1}) are the amounts of Cr(VI) adsorbed on unit mass of the adsorbent when the concentration is at equilibrium and at time t (min), respectively; k_2 (g mg^{-1} min^{-1}) is the rate constant of the pseudo-second-order kinetic model.

Moreover, the well-known linear form of the Langmuir adsorption isotherm (eqn (4)), was used for visual examination of the applicability of the Langmuir model for the adsorption system studied.

$$\frac{C_e}{q_e} = \frac{1}{q_m b} + \frac{C_e}{q_m} \quad (4)$$

where, q_e is the amount adsorbed per unit mass of adsorbent (mg g^{-1}). q_m is the monolayer adsorption capacity (mg g^{-1}) and b is the adsorption desorption equilibrium constant (L mg^{-1}).

3. Results and discussion

3.1 Morphology and structural properties of the obtained Al_2O_3 materials

The high surface area Al_2O_3 materials were prepared through a hydrothermal route followed by a calcination process using aluminum nitrate as precursor and urea as precipitating agent without any template. The microstructures, morphologies and textural properties of the resulting materials were characterized by thermogravimetric and differential scanning calorimetry analyses (TG-DSC), X-ray diffraction (XRD), scanning electron microscopy (SEM), transmission electron microscopy (TEM) and N_2 adsorption–desorption techniques (Fig. 1).

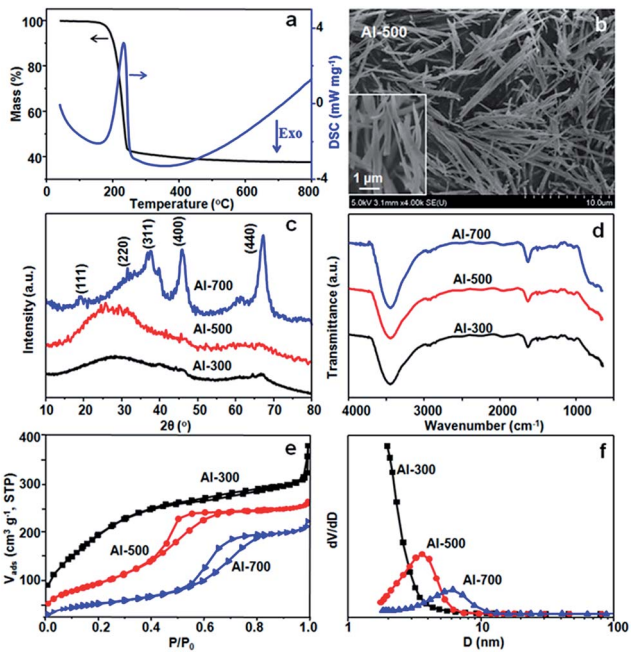

Fig. 1 (a) TG-DSC curves of the hydrothermally synthesized alumina precursor; (b) SEM images of representative sample Al-500; (c) XRD patterns, (d) FT-IR curves, (e) nitrogen adsorption–desorption isotherms and (f) pore size distribution curves of the obtained samples.

The TG-DSC analysis of the hydrothermally synthesized alumina precursor is shown in Fig. 1a. As it can be seen, the TG curve displays three major weight losses. The first weight loss below 175 °C is assigned to the loss of physically adsorbed water. The second one between 175 and 245 °C is mainly associated with the decomposition of $NH_4[Al(OOH)HCO_3]$ and release of CO_2, NH_3, and H_2O, *etc.*[30] Finally, the weight loss above 245–500 °C may be related to the release of water resulting from the phase transformation of the amorphous phases to the crystalline phases as well as the combustion of some certain compounds strongly retained on the alumina surface. The TG curve is leveled off at about 500 °C, which means the complete decomposition of the alumina precursors. So in order to shed light onto the effect of the calcination temperatures on the final samples, three different temperatures (300 °C, 500 °C and 700 °C) were chosen and the final products are named as Al-300, Al-500 and Al-700, respectively. The morphology of the representative sample Al-500 was further investigated by SEM, as shown in Fig. 1b. It can be seen that the obtained sample was composed of uniform rods with 2–5 μm in length and 0.2–0.5 μm in diameter.

The effect of calcination temperature on the crystalline phases and pore structures of the alumina were also investigated. The powder XRD patterns (Fig. 1c) of the obtained samples demonstrated that sample Al-300 calcined at 300 °C was amorphous. While, as the calcination temperature increased, Al-500 showed a more stabilized structure[28] and the amorphous alumina was gradually converted into γ-Al_2O_3 (JCPDS no. 10-0425) at the calcination temperature of 700 °C (Fig. 1c). The surface functional groups of the three Al_2O_3 materials were examined by FT-IR spectroscopy (Fig. 1d). The peaks at 3458 cm^{-1} and 1642 cm^{-1} correspond to the stretching and bending vibrations of –OH bands in the alumina as well as physically adsorbed water. The appearance of a peak at 825 cm^{-1} could be attributed to the characteristic band of Al–O–Al.[31] Further, the densities of surface hydroxyl groups of Al-300, Al-500 and Al-700 were also measured according to the reported method[28] and the values were calculated to be 2.56, 2.53 and 1.46 mmol g^{-1}, respectively (Table 1).

The nitrogen sorption isotherms and pore size distributions of the alumina samples are shown in Fig. 1e and f. It can be found that sample Al-300 shows a transition between type-I and -IV curves. While the isotherms of Al-500 and Al-700 are type-IV in the IUPAC classification, indicating the presence of mesopores. Table 1 summarizes the porous textural parameters of the three samples. It is clear that the porous textures of final alumina products can be controlled through tuning the calcinations temperature, *i.e.*, the specific surface area from 192 to 773 m^2 g^{-1}. As shown, Al-300 and Al-500 exhibited a higher specific surface area of 773 m^2 g^{-1} and 347 m^2 g^{-1}, respectively, which are higher than that of most reported alumina materials in literature.[23,24,32,33]

Here, taking multiple factors (*e.g.*, thermal stability, surface chemistry and porous structure) into consideration, samples Al-500 and Al-700 were used as adsorbents for further study of their Cr(VI) removal performance. Based on the above results, the obtained Al_2O_3 materials equipped with high surface area,

Table 1 Structural parameters and density of hydroxyl groups of the obtained samples

Sample	S_{BET} (m^2 g^{-1})[a]	V_{total} (cm^3 g^{-1})[b]	D_{peak} (nm)[c]	Density of hydroxyl groups (mmol g^{-1})[d]
A1-300	773	0.48	—	2.56
Al-500	347	0.40	3.6	2.53
Al-700	192	0.34	6.1	1.46

[a] S_{BET} = specific surface area calculated by the Brunauer–Emmett–Teller (BET) method. [b] V_{total} = total pore volume at $P/P_0 = 0.995$. [c] D_{peak} = pore sizes at maxima of the pore size distributions (PSDs). [d] The density of hydroxyl groups is measured *via* a reported fluoride ion adsorption method.

micrometer-sized structure, long aspect ratio, and rich surface hydroxyl groups[28] are considered to provide facile transportation, high adsorption capacity, and easy recovery, which are greatly desired in the removal of pollutants from water.

3.2 Affecting factors on the adsorption of Cr(VI)

3.2.1 Effect of contact time. The removal performance of Cr(VI) using the representative samples Al-500 and Al-700 was evaluated. For these cases, initial concentration of Cr(VI) was of 50 mg L^{-1} and adsorbent dose was 2 g L^{-1}. The pH of initial solution was 3. Fig. 2 shows the effect of contact time on the Cr(VI) removal efficiency of the Al_2O_3 adsorbents.

It is clear from this figure that the removal of Cr(VI) of two samples is rapid in the initial stages (the first 30 min) and becomes slower gradually, and then at the equilibrium stage and thereafter, there is no significant increment in removal. The time of equilibrium was about 3 h for sample Al-500 with a high removal efficiency of 98.6% at 24 h, much higher than that of Al-700 at the same adsorption time. This may be because the calcination temperature of 700 °C for Al-700 was too high and it killed some surface hydroxyl groups. Consequently, the density of hydroxyl groups of Al-700 rapidly dropped to 1.46 mmol g^{-1} from 2.53 mmol g^{-1} of Al-500. So finally, the removal efficiency of Al-500 is much better than Al-700, which may be due to the synergistic effect of its suitable mesoporous structure, high surface area (347 m^2 g^{-1}) and abundant surface hydroxyl groups of Al-500. Hence, sample A1-500 was chosen for further investigation of external factors that influence the Cr(VI) removal efficiency, including the pH, adsorbent dose and initial concentration of Cr(VI).

3.2.2 Effect of pH. It is known that the pH determines the chemistry of Cr(VI) and surface charge of an adsorbent in aqueous solution.[34,35] The initial 25 mg L^{-1} Cr(VI) solution used here is tested to be acidic with pH of ~5.1. At a low pH value, the Al_2O_3 surface is highly protonated and hence favours adsorption of Cr(VI) ions which mainly exist in the form of $HCrO_4^-$ or $Cr_2O_7^-$. The surface protonation degree should reduce with an increase in pH, leading to a decrease of adsorption capacity. Above all, in order to find out the optimum pH for the maximum removal efficiency, the effect of pH on adsorption was examined at 24 h contact time in different pH ranging from 2.0 to 5.0.

Fig. 3 reveals that the Cr(VI) removal efficiency is strongly pH dependent. The maximum adsorption efficiency was achieved at a pH of 3 with a Cr(VI) removal efficiency of 99.8%. As the pH value is above 3.0, the removal efficiency rapidly decline and is only 65.1% at pH of 5.0. It's known that the surface of the Al-500 with a net positive charge can attract the negatively charged $HCrO_4^-$ and $Cr_2O_7^{2-}$ species (dominant species of Cr(VI) at pH <6.5) through electrostatic interactions.[36,37] Under acidic conditions, the surface of the adsorbent becomes highly protonated and favours the uptake of Cr(VI) species in the anionic form. With increase in pH, the degree of protonation of the surface reduces gradually and hence adsorption is decreased. Thus, a more efficient adsorption performance observed at lower pH can be assigned to the gradual increase in attraction between positively charged adsorbent surface and the negatively charged Cr(VI) anionic species. It should be noted that the mass loss of Al-500 during the adsorption process at different pH values could be ignored. Thus, the pH of the solution was adjusted to 3 in the following experiments.

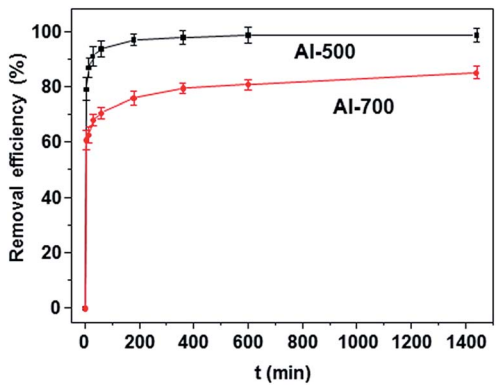

Fig. 2 Effect of time on the removal efficiency of Cr(VI).

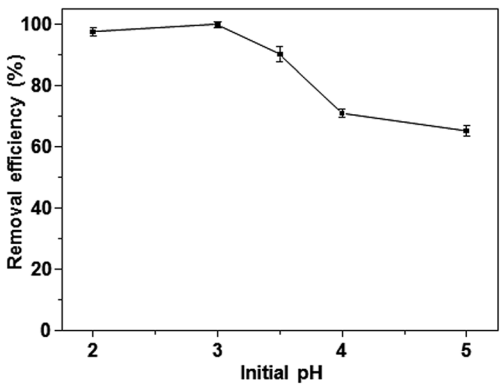

Fig. 3 Effect of pH on the removal efficiency of Cr(VI).

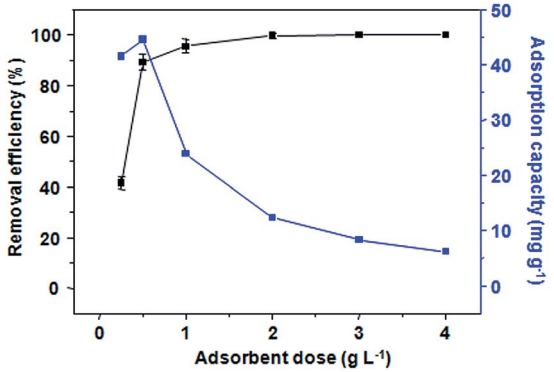

Fig. 4 Effect of the adsorbent dose on Cr(VI) removal using Al-500 with an initial Cr(VI) concentration of 25 mg L^{-1} at pH 3.

3.2.3 Effect of the adsorbent dose. To optimize the adsorbent dose on the adsorption of Cr(VI) from the solution, adsorption experiments were carried out by changing the adsorbent dose at an initial Cr(VI) concentration of 25 mg L^{-1} for 24 h at pH 3. As shown in Fig. 4, the adsorption capacity on per mass of adsorbent reached the highest by using 0.5 g L^{-1} adsorbent. It can also be seen that the removal efficiency increased from 41.6% to 100% by increasing the adsorbent dose from 0.25 to 4 g L^{-1} respectively. This can be attributed to a greater number of active sites for adsorption. The efficiency of Al-500 with 2 g L^{-1} for Cr(VI) was 99.8% after 24 h and the corresponding residual concentration was 0.05 mg L^{-1}. This value is below the guideline set by the Food and Agriculture Organization of the United Nations (FAO) and the World Health Organization (WHO) for of Cr(VI) in drinking water (0.05 mg L^{-1}).[3,4] Thus 2 g L^{-1} of adsorbent is sufficient for the removal of Cr(VI).

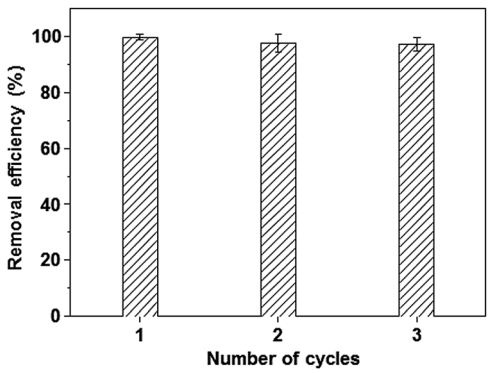

Fig. 5 Cr(VI) removal efficiency over three cycles.

3.2.4 Recyclability. For practical applications, the recyclability of the adsorbent is extremely important.[38] Thus, a preliminary study about the recyclability of the obtained Al_2O_3 adsorbents was carried out. Fig. 5 shows the adsorption–regeneration cycles of Al-500. It is clear that after 3 consecutive operations, the adsorption capacity of Al-500 is 97.6% that of the fresh Al-500. This result shows that sample Al-500 could be repeatedly used as an efficient adsorbent in waste water treatment.

3.3 Adsorption kinetics

The kinetics of Cr(VI) adsorption was studied from the contact time *versus* removal efficiency at different initial Cr(VI) concentrations from 10 mg L^{-1} to 100 mg L^{-1} at pH 3 with 2 g L^{-1} of adsorbent (Fig. 6a).[39] The initial adsorptive concentration provides the necessary driving force to overcome all mass transfer resistances of metal ions between the aqueous and solid phases.[40,41] It is obvious that the removal efficiency of Cr(VI) declines with increasing of initial Cr(VI) concentration. When the initial concentration is less than 50 mg L^{-1}, the removal efficiency close to ~100% is almost unchanged. However, the removal efficiency rapidly decreases when the initial concentration is more than 50 mg L^{-1}. This may be due to that the Cr(VI) adsorption occurs at a limited number of specific surface active sites. At low concentration the large surface area of Al_2O_3 is enough for providing abundant Cr(VI) adsorption sites. While, when the initial concentration becomes higher, the removal efficiency will decline because the available sites of adsorption may not afford the increasing initial amount of Cr(VI).

Here, Ho's pseudo-second-order model[42,43] was employed to study the adsorption process for Cr(VI), as expressed by eqn (3)

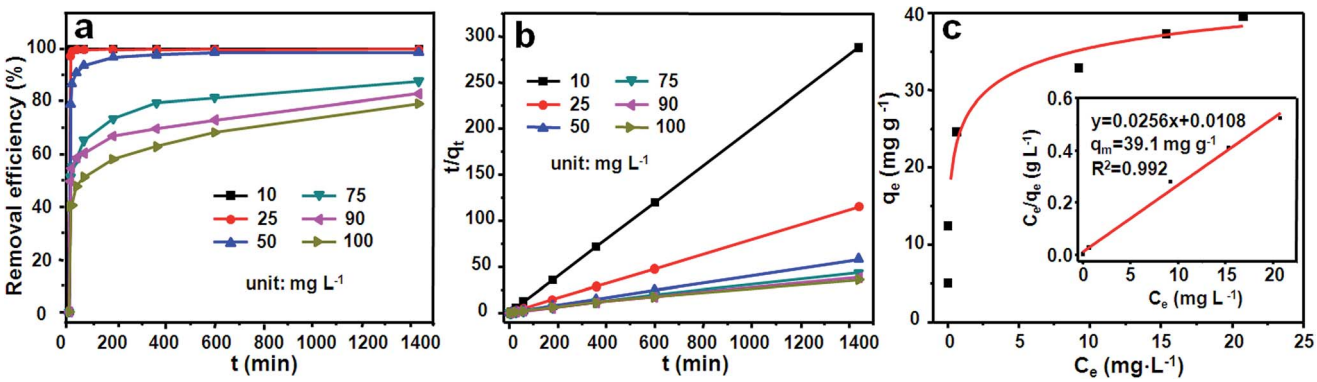

Fig. 6 (a) Effect of contact time on the removal of Cr(VI) on Al-500 at different initial Cr(VI) concentrations; (b) pseudo-second-order kinetic plots for the removal of Cr(VI) on Al-500; (c) Cr(VI) adsorption isotherm (inset C_e/q_e *versus* C_e plot).

Table 2 Kinetic parameters for the adsorption of Cr(VI) by Al-500 based on the pseudo-second-order model

		Pseudo-second-order kinetic model		
C_0 (mg L^{-1})	q_{eexp} (mg g^{-1})	q_{ecal} (mg g^{-1})	k_2 (g mg^{-1} min^{-1})	R^2
10	5.0	5.0	28.17	1.000
25	12.5	12.5	2.24	1.000
50	24.6	24.7	0.012	1.000
75	32.9	33.0	0.0014	0.999
90	37.3	37.4	0.00099	0.997
100	39.6	39.7	0.00062	0.993

in experimental section. Fig. 6b showed the adsorption kinetic plots. The values of q_e and k_2 can be determined from the slope and intercept of the plot, respectively and are shown in Table 2. The q_e is the amount of Cr(VI) adsorbed on unit mass of the adsorbent when the adsorption reaches equilibrium and k_2 is the rate constant of the pseudo-second-order kinetic model. It can be seen that the adsorption kinetics fit well with the pseudo-second-order model (R^2 > 0.990), indicating the adsorption process of Cr(VI) on the Al-500 involves a chemisorption process which is the rate-limiting step.[44]

Moreover, the well-known linear form of the Langmuir adsorption isotherm, eqn (4), was used for visual examination of the applicability of the Langmuir model for the adsorption system studied. It is clear from the inset of Fig. 6c that the experimental data conforms well to the Langmuir equation (R^2 = 0.992), indicating the removal of Cr(VI) was through a monolayer coverage on the surface of the Al-500 adsorbent.[45] Moreover, the constant q_m, which would be important for scaling up the removal process, can be as much as 39.1 mg g^{-1}, which is much higher than most of the reported alumina and/or metal oxides adsorbents (Table 3). This can be attributed to the large surface area (347 m^2 g^{-1}), abundant surface hydroxyl groups and unique rod-like structure of the alumina adsorbents.

3.4 Insight into the adsorption mechanism

In order to better understand the adsorbate–adsorbent systems, XPS and FT-IR were also used to characterize the surface states of the rod-like Al_2O_3 adsorbents before and after adsorption of Cr(VI) ions. Fig. 7a showed full-range XPS spectra of Al-500 before and after Cr(VI) adsorption. Cr information appeared after Cr(VI) were adsorbed on the rod-like Al_2O_3 adsorbent. A high-resolution Cr 2p spectra after Cr(VI) (Fig. 7b) showed two peaks located at 576.3 eV and 585.7 eV, which can be attributed to Cr $2p_{3/2}$ and Cr $2p_{1/2}$ orbitals, respectively.[47] The results indicated that Cr(VI) was adsorbed on the surface of the rod-like Al_2O_3 nanostructures. The FT-IR spectra (Scheme 1 inset) of Al-500-Cr after adsorbing Cr(VI) showed a new peak at 1030 cm^{-1} corresponding to asymmetric stretching vibrations of the Cr=O bond for adsorbed chromium, in agreement with earlier observations,[49] and confirms that Cr(VI) has been adsorbed on the alumina adsorbent surface.

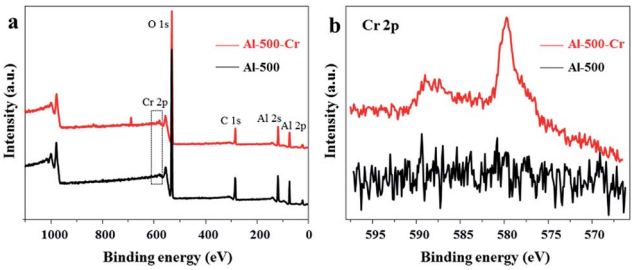

Fig. 7 (a) Full-range XPS spectra and (b) Cr 2p XPS spectra of pristine adsorbents Al-500 and Al-500-Cr after Cr(VI) adsorption.

It is well known that the adsorption at the liquid/solid interface is generally thought to be an ion exchange between metal oxide surface and chromium anions.[47] That is, the adsorption of anions is based on the reaction between anions and the –MOH or $–MOH_2^+$ on the adsorbent surface.[50–52] Hence, the large surface area and abundant hydroxyl groups on the surface of the adsorbent may play a crucial role in the adsorption process of Cr(VI) in aqueous solution. As seen from Scheme 1, when alumina is suspended in water, hydroxyl groups on the surface of Al-500, in the form of Al–OH *via* the dissociation of water,[9,53] can be protonated to form $Al–OH_2^+$ groups under acidic conditions (stage 1). Meanwhile, the Cr(VI) predominates as $HCrO_4^-$ or $Cr_2O_7^{2-}$ species showing negatively charged property at pH <6.5.[36,37] The electrostatic attraction between

Table 3 Comparison of adsorption capacity (q_m) of various adsorbents for Cr(VI) removal

Adsorbents	Adsorbent dose (g L^{-1})	pH	q_m (mg g^{-1})	Ref.
Hierarchical γ-Al_2O_3	0.8	3	6.7	23
Nano-Al_2O_3	NG	2	8.563	24
Polypyrrole/attapulgite	2.0	NG	48.45	34
Activated alumina	10.0	4	7.44	46
3D flowerlike Fe_2O_3	0.4	3	30.0	47
CeO_2 hollow nanospheres	2.0	3	15.4	48
Al_2O_3 rods (Al-500)	2.0	3	39.1	This work

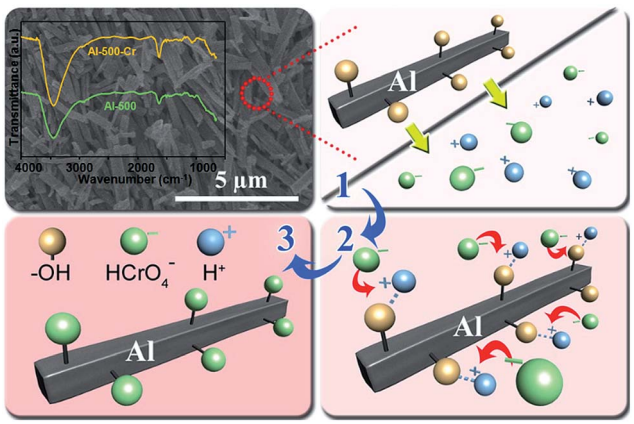

Scheme 1 The adsorption mechanism of alumina for Cr(VI).

positively charged Al_2O_3 samples and negatively charged Cr(VI) species was the initial driving force to bind the anions onto the surface of the adsorbents. Thus the adsorption of Cr(VI) takes place between Al–OH_2^+ of Al_2O_3 adsorbent and chromium anions through the electrostatic interaction and subsequent ion-exchange process (stage 2 and 3).

Generally, the protonation is considered to be a proton-consuming reaction and should increase the pH values of the solution.[54] This has been confirmed in our experiment. Typically, the equilibrium solution pH was found to increase. In the present study, as prolongs the adsorption time, the pH value increases from 3.0 to 6.0 of the equilibrium solution. On the basis of the above results, it can be concluded that the adsorption mechanism of alumina for Cr(VI) was ion exchange between hydroxyl groups on the surface of the Al_2O_3 and Cr(VI) species. The hydroxyl groups played critical roles for Cr(VI) adsorption.

4. Conclusions

We produced rod-like Al_2O_3 materials through a template-free hydrothermal process and subsequent calcination. The pore structure, density of surface hydroxyl groups and amorphous & crystalline types of the final Al_2O_3 products can be tuned through controlling the calcination temperature from 300 °C to 700 °C. Adsorption tests demonstrated that these materials exhibited an excellent Cr(VI) removal performance with the maximum adsorption capacity of 39.1 mg g^{-1}, which is superior to most previously reported alumina adsorbents. The further study showed that the ion-exchange between Cr(VI) species and hydroxyl groups on the surface of alumina played a crucial role in the adsorption process. Importantly, the preliminary cycling experiment showed that the alumina can be easily recovered and displayed an excellent cyclic stability. The combined results demonstrate that these alumina can be considered as an optimum material for the removal of Cr(VI) from aqueous solution.

Acknowledgements

The project was supported by the Special Program for Basic Research of the Ministry of Science and Technology (2013CB934104) and National Natural Science Foundation of China (U1462120).

Notes and references

1 S. S. Gupta and K. G. Bhattacharyya, *RSC Adv.*, 2014, **4**, 28537–28586.
2 X. Li, R. Zhao, B. Sun, X. Lu, C. Zhang, Z. Wang and C. Wang, *RSC Adv.*, 2014, **4**, 42376–42382.
3 A. Mahapatra, B. G. Mishra and G. T. Hota, *Ind. Eng. Chem. Res.*, 2013, **52**, 1554–1561.
4 G. F. Nordberg, B. A. Fowler, M. Nordberg and L. T. Friberg, *Handbook on the toxicology of metals*, Academic Press, Burlington, 2007.
5 S. J. Fuller, D. I. Stewart and I. T. Burke, *Ind. Eng. Chem. Res.*, 2013, **52**, 4704–4714.
6 Y. Xu, J. Zhang, G. Qian, Z. Ren, Z. Xu, Y. Wu, Q. Liu and S. Qiao, *Ind. Eng. Chem. Res.*, 2010, **49**, 2752–2758.
7 M. Bhaumik, A. Maity, V. V. Srinivasu and M. S. Onyango, *J. Hazard. Mater.*, 2011, **190**, 381–390.
8 Y. Wu, X. Ma, M. Feng and M. Liu, *J. Hazard. Mater.*, 2008, **159**, 380–384.
9 Y. Wang, G. Wang, H. Wang, W. Cai, C. Liang and L. Zhang, *Nanotechnology*, 2009, **20**, 155604–155609.
10 C. Han, W. Cai, W. Tang, G. Wang and C. Liang, *J. Mater. Chem.*, 2011, **21**, 11188–11196.
11 Y. Lin, W. Cai, X. Tian, X. Liu, G. Wang and C. Liang, *J. Mater. Chem.*, 2011, **21**, 991–997.
12 D.-H. Liu, Y. Guo, L.-H. Zhang, W.-C. Li, T. Sun and A.-H. Lu, *Small*, 2013, **9**, 3852–3857.
13 M. L. Paul, J. Samuel, S. B. Das, S. Swaroop, N. Chandrasekaran and A. Mukherjee, *Ind. Eng. Chem. Res.*, 2012, **51**, 15242–15250.
14 L. Zhang, X. Jiao, D. Chen and M. Jiao, *Eur. J. Inorg. Chem.*, 2011, **2011**, 5258–5264.
15 L.-S. Zhong, J.-S. Hu, H.-P. Liang, A.-M. Cao, W.-G. Song and L.-J. Wan, *Adv. Mater.*, 2006, **18**, 2426–2431.
16 S. R. Chowdhury, E. K. Yanful and A. R. Pratt, *J. Hazard. Mater.*, 2012, **246**, 235–236.
17 J.-S. Hu, L.-S. Zhong, W.-G. Song and L.-J. Wan, *Adv. Mater.*, 2008, **20**, 2977–2982.
18 L.-S. Zhong, J.-S. Hu, A.-M. Cao, Q. Liu, W.-G. Song and L.-J. Wan, *Chem. Mater.*, 2007, **19**, 1648–1655.
19 S. Recillas, J. Colón, E. Casals, E. González, V. Puntes, A. Sánchez and X. Font, *J. Hazard. Mater.*, 2010, **184**, 425–431.
20 S. Asuha, X. G. Zhou and S. Zhao, *J. Hazard. Mater.*, 2010, **181**, 204–210.
21 W. Li, C.-Y. Cao, L.-Y. Wu, M.-F. Ge and W.-G. Song, *J. Hazard. Mater.*, 2011, **198**, 143–150.
22 F. Granados-Correa and J. Jiménez-Becerril, *J. Hazard. Mater.*, 2009, **162**, 1178–1184.
23 W. Cai, J. Yu and M. Jaroniec, *J. Mater. Chem.*, 2010, **20**, 4587–4594.
24 Y. C. Sharma, V. Srivastava and A. K. Mukherjee, *J. Chem. Eng. Data*, 2010, **55**, 2390–2398.
25 A.-F. An, A.-H. Lu, Q. Sun, J. Wang and W.-C. Li, *Gold Bull.*, 2011, **44**, 217–222.
26 J. Wang, A.-H. Lu, M. Li, W. Zhang, Y.-S. Chen, D.-X. Tian and W.-C. Li, *ACS Nano*, 2013, **7**, 4902–4910.
27 J. Wang, K. Shang, Y. Guo and W.-C. Li, *Microporous Mesoporous Mater.*, 2013, **181**, 141–145.
28 N. Kawasaki, F. Ogata and H. Tominaga, *J. Hazard. Mater.*, 2010, **181**, 574–579.
29 M. Baikousi, A. B. Bourlinos, A. Douvalis, T. Bakas, D. F. Anagnostopoulos, J. Tuček, K. Šafářová, R. Zboril and M. A. Karakassides, *Langmuir*, 2012, **28**, 3918–3930.
30 P. Bai, F. Su, P. Wu, L. Wang, F. Y. Lee, L. Lv, Z. Yan and X. S. Zhao, *Langmuir*, 2007, **23**, 4599–4605.
31 A. L. Ahmad and N. N. N. Mustafa, *Int. J. Hydrogen Energy*, 2007, **32**, 2010–2021.

32 Y. J. O. Asencios and M. R. Sun-Kou, *Appl. Surf. Sci.*, 2012, **258**, 10002–10011.
33 M. Akia, S. M. Alavi, M. Rezaei and Z.-F. Yan, *J. Porous Mater.*, 2010, **17**, 85–90.
34 Y. Chen, H. Xu, S. Wang and L. Kang, *RSC Adv.*, 2014, **4**, 17805–17811.
35 P. Pommerenk and G. C. Schafran, *Environ. Sci. Technol.*, 2005, **39**, 6429–6434.
36 S. Zink, R. Schoenberg and M. Staubwasser, *Geochim. Cosmochim. Acta*, 2010, **74**, 5729–5745.
37 G. Lee, C. Chen, S.-T. Yang and W.-S. Ahn, *Microporous Mesoporous Mater.*, 2010, **127**, 152–156.
38 K.-H. Goh, T.-T. Lim and Z. Dong, *Water Res.*, 2008, **42**, 1343–1368.
39 Y. S. Ho and G. Mckay, *Water Res.*, 1999, **33**, 578–584.
40 G. Dönmez and Z. Aksu, *Process Biochem.*, 2002, **38**, 751–762.
41 S. Larous, A.-H. Meniai and M. Bencheikh Lehocine, *Desalination*, 2005, **185**, 483–490.
42 Y. S. Ho and G. Mackay, *Process Biochem.*, 1999, **34**, 451–465.
43 S. Azizian, *J. Colloid Interface Sci.*, 2004, **276**, 47–52.
44 M. Ahmaruzzaman, *Adv. Colloid Interface Sci.*, 2011, **166**, 36–59.
45 I. Langmuir, *J. Am. Chem. Soc.*, 1918, **40**, 1361–1403.
46 S. Mor, K. Ravindra and N. R. Bishnoi, *Bioresour. Technol.*, 2007, **98**, 954–957.
47 C.-Y. Cao, J. Qu, W.-S. Yan, J.-F. Zhu, Z.-Y. Wu and W.-G. Song, *Langmuir*, 2012, **28**, 4573–4579.
48 C.-Y. Cao, Z.-M. Cui, C.-Q. Chen, W.-G. Song and W. Cai, *J. Phys. Chem. C*, 2010, **114**, 9865–9870.
49 M. A. Vuurman, I. E. Wachs, D. J. Stufkens and A. Oskam, *J. Mol. Catal.*, 1993, **80**, 209–227.
50 S. A. Wasay, S. Tokunaga and S.-W. Park, *Sep. Sci. Technol.*, 1996, **31**, 1501.
51 C. Namasivayam and S. Senthikumar, *Ind. Eng. Chem. Res.*, 1998, **37**, 4816–4822.
52 S. Tokunaga, S. A. Wasay and S.-W. Park, *Water Sci. Technol.*, 1997, **35**, 71–78.
53 F. Ogata, N. Kawasaki, T. Nakamura and S. Tanada, *J. Colloid Interface Sci.*, 2006, **300**, 88–93.
54 Y. Lin, W. Cai, H. He, X. Wang and G. Wang, *RSC Adv.*, 2012, **2**, 1769–1773.